Journal of Medicinal Chemistry

ARTICLE

pubs.acs.org/jmc

In Vivo PET Imaging of Histone Deacetylases by ^{18}F-Suberoylanilide Hydroxamic Acid (^{18}F-SAHA)

J. Adam Hendricks,[†] Edmund J. Keliher,[†] Brett Marinelli, Thomas Reiner, Ralph Weissleder,* and Ralph Mazitschek*

Center for Systems Biology, Massachusetts General Hospital and Harvard Medical School, 185 Cambridge Street, Massachusetts 02114, United States

Supporting Information

ABSTRACT: Histone deacetylases (HDACs) are a group of enzymes that modulate gene expression and cell state by deacetylation of both histone and non-histone proteins. A variety of HDAC inhibitors (HDACi) have already undergone clinical testing in cancer. Real-time in vivo imaging of HDACs and their inhibition would be invaluable; however, the development of appropriate imaging agents has remained a major challenge. Here, we describe the development and evaluation of ^{18}F-suberoylanilide hydroxamic acid (^{18}F-SAHA **1a**), a close analogue of the most clinically relevant HDAC inhibitor suberoylanilide hydroxamic acid (SAHA). We demonstrate that **1a** has near identical biochemical activity profiles to that of SAHA and report findings from pharmacokinetic studies. Using a murine ovarian cancer model, we likewise show that HDAC inhibitor target binding efficacy can be quantitated within 24 h of administration. **1a** thus represents the first ^{18}F-positron emission tomography (PET) HDAC imaging agent, which also exhibits low nanomolar potency and is pharmacologically analogous to a clinically relevant HDAC inhibitor.

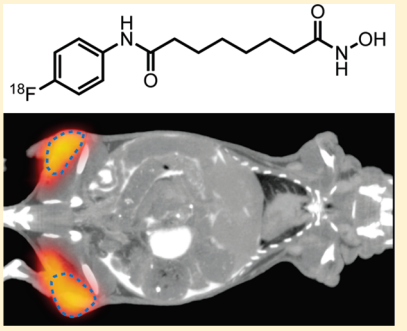

INTRODUCTION

Histone deacetylases (HDACs) are enzymatic components of chromatin modifying complexes and modulate gene expression via interactions with transcriptional regulatory proteins and via modification of the amino-terminal histone tail lysine residues.[1,2] More recently a considerable number of non-histone protein substrates have also been identified, indicating that lysine acetylation represents a post-translational modification with broad regulatory significance.[3] To date, 18 different HDACs have been characterized and, based on their phylogeny, grouped into four major classes.[4] Class I (HDAC1−3,8), class II (HDAC4−7,9), and class IV (HDAC11) are zinc-dependent hydrolases that are formally referred to as HDACs. In contrast, class III (Sirt1−7) enzymes, the sirtuins, function by a catalytically distinct, NAD^+-dependent mechanism. While the enzymatic activities of HDAC isoforms overlap in vitro, their biological activity and substrate selectivities in vivo are typically regulated by specific multiprotein binding partners, as well as by their unique tissue and cellular distribution.

The first HDAC inhibitors (HDACi) were developed for cancer applications following findings that they induce apoptosis and differentiation in malignant cell lines.[5,6] Thus far, two chemically distinct HDACi, suberoylanilide hydroxamic acid (SAHA) **2** (Vorinostat, Merck Research Laboratories) and the more recently developed microbial natural product FK228 **3** (Romidepsin, Celgene),[2] have received FDA approval for the treatment of specific T-cell malignancies (Figure 1). In addition, increasing information regarding HDAC function from genetic studies have now elucidated specific roles for different HDAC isoforms in the regulation of fundamental biological processes.[3] Notably, they have been demonstrated to be master regulators of mitosis, cell differentiation, apoptosis,[6] chromatin organization,[7] metabolism,[8] learning and memory,[9] and the immune response.[10] Given the relevance that most of these critical cellular functions have to disease, small molecule modulators of chromatin modifying enzymes are now being developed, not only for oncological applications but more broadly for the treatment of psychiatric, immunological, neuromuscular, inflammatory, metabolic, genetic, and infectious diseases.[2,11,12]

SAHA is a broad spectrum inhibitor that potently targets class I and class II HDAC enzymes.[13] At present, SAHA and other HDACi are being explored as potential drug therapies for a number of different malignancies, both as single agents and in combination with other agents.[2,12,14] A critical bottleneck in the clinical development and use of HDACi has been the inability to rapidly quantitate target inhibition in the clinic. Acetylation of peripheral mononuclear cells initially showed early promise as a potential biomarker but ultimately failed to correlate with clinical response in patients.[15] Conversely, conventional anatomic imaging modalities used to monitor clinical response are only capable of reporting on tumor size or on rudimentary physiologic changes such as alterations in perfusion, both of which occur relatively late after treatment onset. In vivo imaging of HDAC

Received: May 21, 2011
Published: July 01, 2011

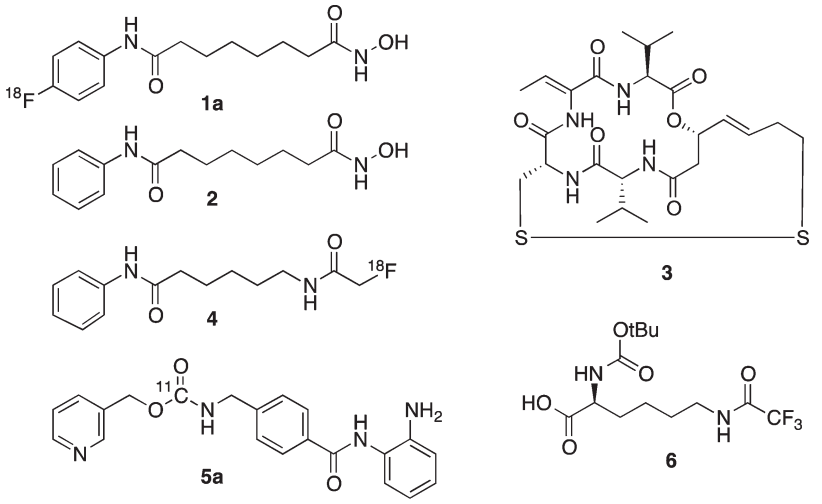

Figure 1. Structures of HDAC inhibitors and HDAC imaging agents.

Scheme 1. Synthesis of 1b[a]

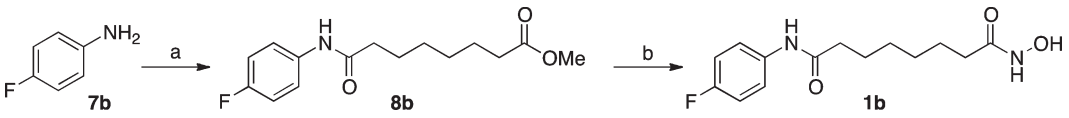

[a] (a) Methyl 8-chloro-8-oxooctanoate, Et_3N, CH_2Cl_2, room temp, 1 h, 54%; (b) 50% NH_2OH (aq), 1 N NaOH(MeOH), room temp, 12 h, 65%.

proteins (and to some degree their activity state) has likewise been rudimentary at best and, as such, detailed analyses have been limited to readily accessible tissue specimens, which can only be analyzed using ex vivo techniques. Thus, in order to investigate the efficiency of existing and novel HDACi, there is a clear need for imaging probes. Moreover, imaging of HDACs may provide important basic scientific insights, which could lead to novel clinical applications.

To date, only a few compounds for in vivo HDAC imaging have been reported. Reid et al., for example, developed 6-([^{18}F]fluoroacetamide)-1-hexanoicanilide (FAHA) **4** for cerebral imaging. **4** is a ^{18}F-functionalized hybrid of the HDAC inhibitor SAHA, an acetyl lysine mimic that lacks the hydroxamate chelator, which is required for potent target binding.[16] Furthermore, **4**, which features a reactive fluoro ketone and resembles an HDAC substrate rather than an inhibitor, is rapidly metabolized in vivo, thus complicating imaging and analysis. More recently the development of [^{11}C]MS-275 **5a**, a carbon-11-labeled version of the benzamide class HDAC inhibitor MS-275 (entinostat, Syndax Pharmaceuticals) **5b**, has been reported for cerebral imaging.[17] **5b**, as most benzamide based HDAC inhibitors, is selective for HDAC1−3, albeit 20- to 70-fold less potent than SAHA.[13] Unfortunately, the blood−brain barrier penetration of **5a** was found to be unsuitable for the intended studies and competition with cold **5b** failed to demonstrate specific binding.[17] Further, the short half-life of carbon-11 (∼20 min) compared to fluorine-18 (∼110 min) imposes technical challenges and limits potential applications. Another study by Ronen and co-workers investigated the use of Boc-lysine trifluoroacetic acid **6** (BLT) as a substrate for HDACs, using ^{19}F magnetic resonance spectroscopy.[18] Trifluoroacetyl-lysine-based substrates, however, are not suitable for all HDACs because they exhibit large variations in their specificity for individual HDAC isoforms. For example, the principal enzymes that metabolize BLT are HDAC8 and (to a lesser degree) class IIa HDACs. In contrast, current clinical HDAC inhibitor candidates primarily target HDACs 1, 2, 3, and 6.[13,19]

RESULTS AND DISCUSSION

Here we describe the development of an in vivo PET imaging agent with strong similarities in pharmacology, potency, and isoform selectivity to SAHA, the most clinically relevant HDAC inhibitor. Introduction of an ^{18}F label to the 4-position of the aromatic ring of SAHA (^{18}F-SAHA **1a**) appeared to be the most practical approach. To first determine that this functionalization would not negatively impact the compound's biological activity, we synthesized and profiled ^{19}F-SAHA **1b** against HDACs 1−9. The synthesis was readily accomplished by following reported strategies, with minor modification (Scheme 1).[20] Synthesis began with acylation of the commercially available 4-fluoroaniline **7b**, with suberic chloride methyl ester. Subsequent treatment with basic hydroxylamine resulted in the conversion of the methyl ester **8b** to the hydroxamic acid.

The biochemical profiling of **1b** against purified HDAC isoforms demonstrated that **1b**, as expected, inhibited only HDACs 1−3 and 6.[13] Moreover, inhibition of these primary HDAC targets by **1b** exhibited a potency and selectivity virtually indistinguishable from SAHA itself. This finding thus identified **1b** as a promising candidate for the development of a PET imaging probe (Figure 2a).

Our next goal was to develop a reliable synthetic strategy for the routine synthesis of **1a**, which would enable generation of **1a** in quantities sufficient even for large animal studies. Direct fluorination of 1,4-dinitrobenzene **9** with ^{18}F (no carrier added (nca)) under phase transfer conditions and microwave heating

dx.doi.org/10.1021/jm200620f |J. Med. Chem. 2011, 54, 5576–5582

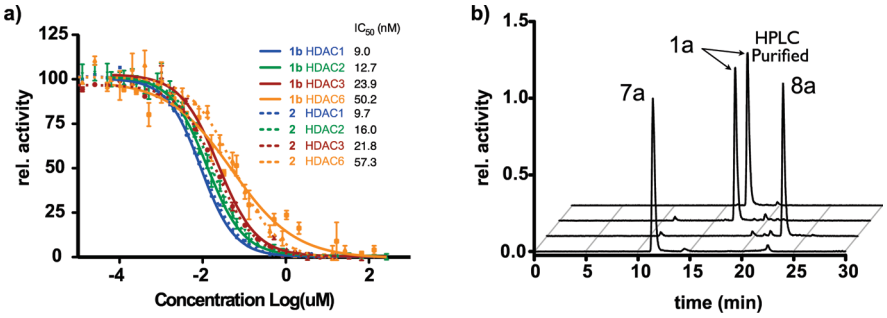

Figure 2. (a) Dose−response profile for **1b** and **2** against HDACs 1−3 and 6. (b) Analytical radio-HPLC traces.

Scheme 2. Synthesis of 1a[a]

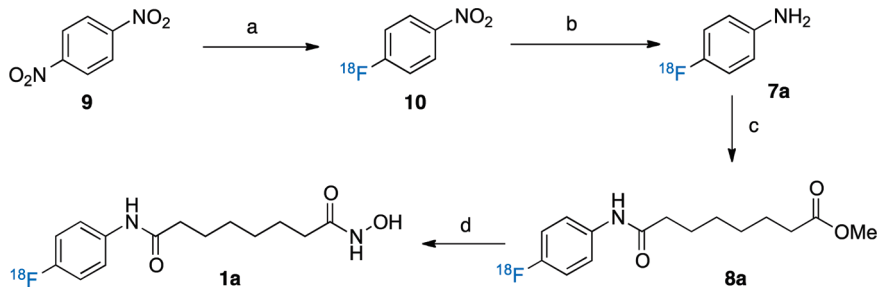

[a] (a) (1) K_2CO_3, K222, $^{18}F^-$ (nca), DMSO, 120 °C, microwave, 5 min; (2) C18 isolation, MeOH elution, 78%; (b) (1) $NaBH_4$, 10% Pd/C, room temp, 10 min; (2) LiChrolut EN isolation, THF elution, Na_2SO_4/Celite drying, 58%; (c) methyl 8-chloro-8-oxooctanoate, room temp, 5 min; (d) (1) 50% NH_2OH (aq), 1 N NaOH(MeOH), room temp, 3 min; (2) HPLC purification, concentration; (3) reconstitution into vehicle (88% two steps).

afforded 1-[^{18}F]fluoro-4-nitrobenze **10** after 5 min at 120 °C. This intermediate was consecutively reduced by catalytic hydrogenation with sodium borohydride and Pd/C to yield 4-[^{18}F]-fluoroaniline **7a**, which was isolated on a LiChrolut EN column.[21] The ^{18}F-labeled aniline was subsequently converted to the desired product via compound **1a**, following the same strategy employed for synthesis of cold **1b** using optimized conditions for radiochemical synthesis (Figure 2b). Overall, this four-step synthesis is remarkably clean, can be carried out in less than 2 h, and affords **1a** with a decay corrected yield of 40%. Following HPLC purification, the radiochemical purity was greater than 98% (Scheme 2). Several alternative routes attempting to introduce the ^{18}F later in the synthesis were explored unsuccessfully.

To date, very little information exists in the published scientific literature on the pharmacokinetic and tissue distribution of SAHA in murine models. Such knowledge, however, is critical for the development of therapeutic applications in central nervous system disorders or spinal muscular atrophy. Thus, following scale-up synthesis and characterization of the radiotracer, we next tested the compound in vivo. Initially, we determined the plasma half-life of **1a** and its tissue distribution. The blood half-life, following a single bolus intravenous injection, was then measured for three commonly utilized pharmacological formulations (A, 60% PEG, 40% water; B, 10% DMSO in water; C, 10% DMAC, 10% Solutol HS15, 80% PBS). All formulations exhibited a biphasic pharmacokinetic profile, with rapid elimination during the first 10 min. The initial $t_{1/2}$ was estimated as less than 1−4 min, mostly through renal clearance, and this was followed by a terminal half-life that was approximately 10 times longer. Notably, the initial half-lives appeared to be strongly dependent on the formulation, but these early time points are generally not captured by traditional liquid chromatography/mass spectrometry (LC/MS) based approaches. Less than 1% of the dosed compound was still present in whole blood when using formulation A (60% PEG400, 40% water), while formulations B (10% DMSO, 90% water) and C (10% dimethylacetamide, 10% Solutol HS15, 80% PBS) resulted in retention of approximate 3% and 6% of the compound, respectively (Figure 3a). Following this initial "burst" phase, elimination half-lives appeared to be equivalent and correlated well with the blood-half-life, as determined by serial in vivo PET imaging (Figure 3d). We also tested oral administration of the compound (formulation C, Figure 3b) and observed similar kinetics as determined by conventional HPLC mass spectrometry.

We subsequently determined the tissue distribution of **1a**. For each experiment, cohorts of mice were sacrificed at 1 and 3 h following intravenous injection of the probe. Tissues were then excised and weighed, and ^{18}F activity was measured. As shown in Figure 3c, **1a** had the highest concentration in the kidney, liver and blood, with relatively low distribution in other tissues (Figures 3c and 4a). Interestingly, cardiac tissue also appeared to have comparatively low concentrations of **1a**, which may in part explain the relatively low cardiotoxicity of SAHA compared to other HDACi. Of all organs investigated, the thymus and brain exhibited the lowest concentration of **1a**, implying that if used to study brain function, SAHA would likely require intrathecal administration.

Upon demonstrating that **1a** exhibits a suitable pharmacological profile, we next assessed whether administration of "cold" SAHA could be used to measure HDAC inhibition in a mouse

dx.doi.org/10.1021/jm200620f |J. Med. Chem. 2011, 54, 5576–5582

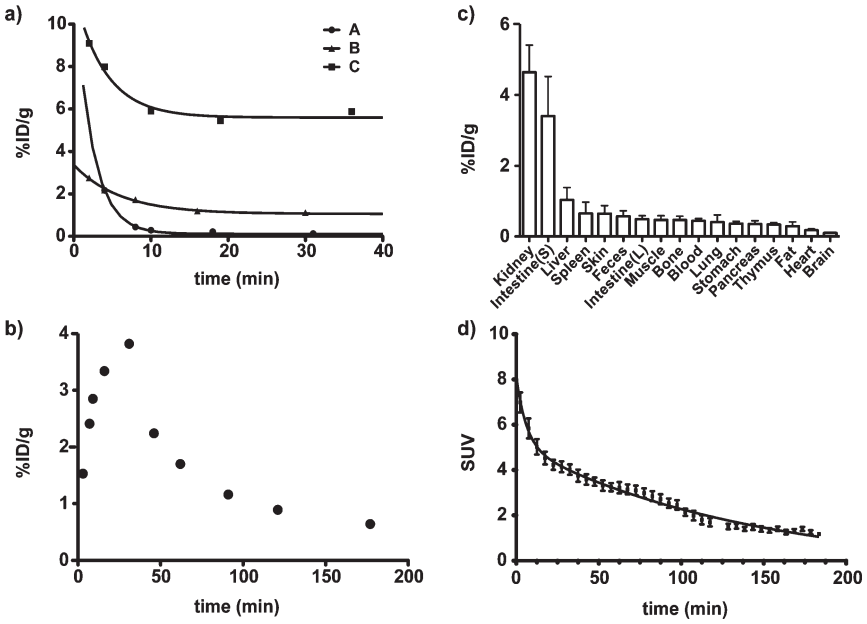

Figure 3. Blood half-life of **1a** following (a) iv and (b) po administration; (c) biodistribution; (d) blood half-life determined by dynamic PET scan. % ID/g is injected dose per gram of tissue. SUV, is standardized uptake value.

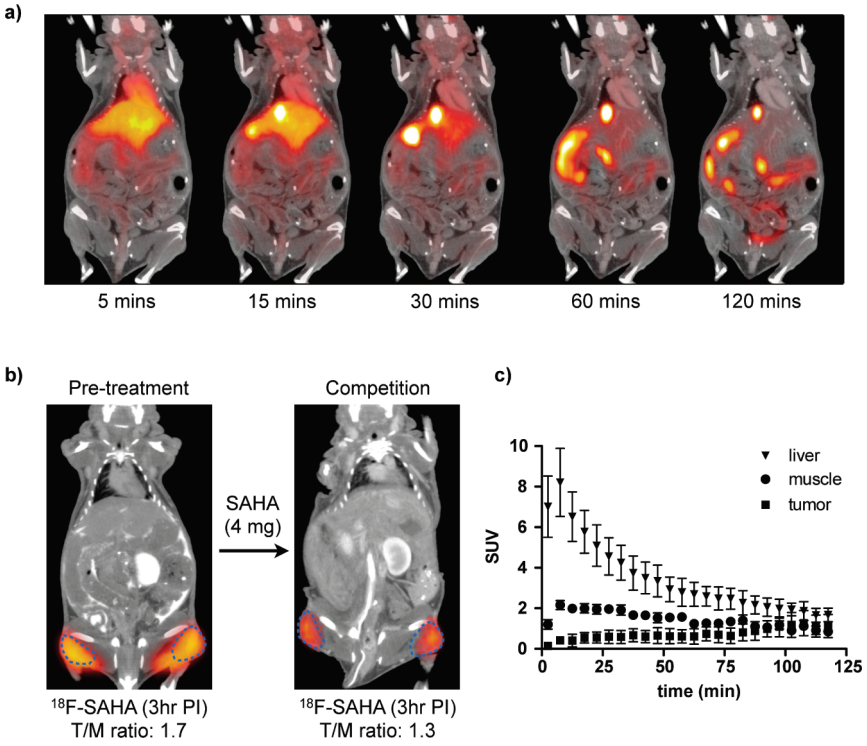

Figure 4. (a) Dynamic PET−CT following iv administration of **1a** in C57BL/6 mouse. (b) PET−CT scan of tumor xenograft before and after competition with "cold" SAHA, where blue dotted line indicates tumor perimeter. (c) Time dependent distribution of **1a**.

model of cancer. Since SAHA is currently undergoing clinical trials for the treatment of ovarian cancer, we selected the A2780 ovarian cancer model for this study. Consistent with class I HDAC expression levels in both malignant and benign tissues (Figure 4c), **1a** was observed to accumulate in tumors in a time-dependent manner, following its systemic administration. To subsequently determine whether **1a** imaging could be used to measure HDAC inhibition in vivo, we performed repeat **1a** PET imaging experiments on a cohort of mice both before and after cold SAHA treatment (2 × 2 mg injection, Figure 4b). As expected for selective competition, the tumor/muscle ratio decreased from 1.7 ± 0.12 to 1.3 ± 0.01 (23%), following two

dx.doi.org/10.1021/jm200620f |J. Med. Chem. 2011, 54, 5576–5582

single doses of cold SAHA treatment in a 24 h period (Figure 4b). These studies thus show proof of principle that **1a** imaging can be used to measure target engagement within 24 h of drug administration. Overall, these studies describe the development of a versatile HDAC PET imaging agent that not only exhibits low nanomolar potency but is also pharmacologically similar to a clinically relevant HDACi. It is likely that this compound will be useful for testing SAHA and other HDACi in the clinic.

EXPERIMENTAL METHODS

Chemistry. Reagents were purchased from Acros, Alfa-Aesar, and Sigma-Aldrich Co. and used without further purification unless otherwise noted. Silica gel 60 was used for purification, 40−63 μm. Proton and carbon nuclear magnetic resonance (^{1}H and ^{13}C NMR) spectra were recorded on a Varian AS-400 (400 MHz) spectrometer. Chemical shifts for protons are reported in parts per million (ppm) and are referenced against the dimethylsulfoxide lock signal (^{1}H, 2.50 ppm; ^{13}C, 39.52 ppm). Data are reported as follows: chemical shift, integration, multiplicity (s = singlet, d = doublet, t = triplet, m = multiplet), and coupling constants (Hz). Preparatory and analytical LC/MS were performed on mass directed autopurification systems from Waters Co. (Milford, MA), operated by Fractionlynx 4.0 or Masslynx software with Waters Xterra columns (C18, 10 μm, 19 mm × 50 mm for preparative; C18, 5 μm, 4.6 mm × 50 mm for analytical). High-resolution mass spectra were acquired on a Bruker Daltonics APEXIV 4.7 T Fourier transform ion cyclotron resonance mass spectrometer (FT-ICR-MS), with ESI (electrospray ion) source. The chemical purity of the target compounds was determined by LC/MS using the following conditions: a Waters SFO/3100 with Waters Xterra C18 column using a binary solvent system (0.1% TFA in water and acetonitrile), with monitoring between 200 and 400 nm. The purity of each compound was ≥95%.

7-(4-Fluorobenzoylamino)heptanoic Acid Methyl Ester 8b. 4-Fluoroaniline **7b** (259 μL, 2.7 mmol) and triethylamine (376 μL, 2.7 mmol) were dissolved in DCM (2 mL) and cooled to 0 °C. To this solution was added methyl suberyl chloride (350 μL, 2.5 mmol). After 1 h the mixture was diluted with DCM (10 mL) and then washed with H_2O (10 mL), brine (10 mL) and then dried with magnesium sulfate. Purification via column chromatography (silica gel, DCM/EtOAc 40%) gave product **8b** (383 mg, 54%). ^{1}H NMR (400 MHz, DMSO-d_6) δ 9.91 (s, 1H), 7.59 (dd, J = 9.2, 5.1 Hz, 2H), 7.12 (t, J = 9.0 Hz, 2H), 3.57 (s, 3H), 2.28 (q, J = 7.5 Hz, 4H), 1.63−1.44 (m, 4H), 1.29 (dd, J = 7.3, 3.6 Hz, 4H). ^{13}C NMR (101 MHz, DMSO-d_6) δ 173.37, 171.09, 157.778 (d, J_{C-F} = 240.4 Hz), 135.77, 120.69 (d, J_{C-F} = 8.1 Hz), 115.20 (d, J_{C-F} = 22.2 Hz), 51.21, 36.24, 33.24, 28.25, 24.94, 24.34. HRMS (ESI) for $C_{15}H_{20}FNO_3$: calculated 282.1500; observed 282.1506 $[M + H]^+$, 304.1332 $[M + Na]^+$.

***N*-Hydroxy-*N*′-(4-fluorophenyl)octanediamide 1b.** Methyl ester **8b** (180 mg, 0.640 mmol) was suspended in a 1:1 (v/v) mixture of methanol and 50% hydroxylamine (aq). To this suspension was added 1 N $NaOH_{(aq)}$ (1.5 mL). After 12 h the mixture had become homogeneous. Then 1 N HCl was added, bringing the solution back to a neutral pH, upon which the product precipitated from solution. Filtration of the white solid afforded the product **6** (84 mg, 65%). ^{1}H NMR (400 MHz, DMSO-d_6) δ 10.34 (s, 1H), 9.92 (s, 1H), 8.67 (s, 1H), 7.59 (dd, J = 9.2, 5.1 Hz, 2H), 7.12 (t, J = 8.9 Hz, 2H), 2.27 (t, J = 7.4 Hz, 2H), 1.93 (t, J = 7.4 Hz, 2H), 1.55 (t, J = 14.5, 7.2 Hz, 2H), 1.47 (t, J = 14.2, 7.2 Hz, 2H), 1.31−1.20 (m, 4H). ^{13}C NMR (101 MHz, DMSO-d_6) δ 171.11, 169.09, 157.78 (d, J_{C-F} = 240.4 Hz), 135.77, 120.70 (d, J_{C-F} = 8.1 Hz), 115.21 (d, J_{C-F} = 22.2 Hz), 36.29, 32.26, 28.43, 25.06, 25.03. HRMS (ESI) for $C_{14}H_{19}FN_2O_3$: calculated 283.1452; observed 283.1444 $[M + H]^+$, 305.11258 $[M + Na]^+$.

Radiochemistry. [^{18}F]Fluoride (nca) in ^{18}O enriched water was purchased from PETNET (Woburn, MA). Solid phase extraction cartridges were purchased from Thermo (HYPERSEP C18, 500 mg, 3 mL) and Merck (LiChrolut EN, 200 mg, 3 mL). Preparative high performance liquid chromatography (HPLC) purification (method A) was achieved using a Machery-Nagel Nucleodur C18 Pyramid 250 mm × 10 mm Vario-Prep column (80:20 (v/v) in water/acetonitrile (MeCN) with 0.1% trifluoroacetic acid at 5.5 mL·min^{-1}), and analytical HPLC (method B) was performed employing a Grace VYDAC (218TP510) C18 reversed-phase column (eluents A = 0.1% TFA (v/v) in water and B = MeCN; gradient 0−17 min, 5−60% B; 17−21 min, 60−95% B; 21−24 min, 95% B; 24−25 min, 95−5% B; 25−30 min, 5% B; 2 mL min^{-1}) with a dual-wavelength UV−vis detector followed by a flow-through γ detector connected in series. Preparative and analytical HPLC analyses of ^{18}F-labeled compounds were calibrated with the corresponding ^{19}F analogues. Microwave synthesis was conducted in a CEM (Matthews, NC) microwave synthesizer operated with Discover software package. Radioactive samples injected into mice were measured using a Capintec 127R dose calibrator. Radioactivity in blood half-life and biodistribution studies was quantified using a Perkin-Elmer Wallac Wizard 3 in. 1480 automatic γ counter.

Synthesis of 1a. A 10 mL microwave test tube was charged with 26.9 ± 2.7 mCi (1.0 GBq) [^{18}F]fluoride (nca), K_2CO_3 (1.38 mg, 10 μmol) in water, 135 μL, Kryptofix 222 (6.8 mg, 18 μmol), and 1 mL of MeCN. Water was removed azeotropically by microwave heating to 98 °C and a flow of argon. Azeotropic drying is repeated by the addition of anhydrous MeCN (4 × 1 mL) at 3 min intervals. After the mixture was cooled to room temperature, 1,4-dinitrobenzene **9** (4 mg, 23.8 μmol) in DMSO (500 μL) was added. The vessel was sealed and heated to 120 °C for 5 min and then cooled to room temperature. The reaction mixture was diluted with water (8 mL) and passed through a C18 cartridge (Thermo, 500 mg, conditioned with 10 mL of EtOH and 2 × 10 mL of water) trapping the 4-[^{18}F]fluoronitrobenzene (**10**). The C18 cartridge was washed with water (5 mL), and 16.1 ± 0.9 mCi (596 MBq) **10** was eluted from the cartridge with MeOH (1 mL) in 78.3 ± 6.4% dcRCY. A 10 μL aliquot was removed for HPLC analysis (method B), **10** t_R = 21.4 min. After addition of 3 mg of Pd/C and 28 mg (740 μmol) of $NaBH_4$, the reaction mixture was stirred at room temperature for 5 min, at which time unreacted $NaBH_4$ was quenched by the addition of 300 μL of 6 N HCl. The mixture was diluted with 1 N $NaOH_{(aq)}$ (8 mL) and passed through a Lichrolut EN cartridge (Merck, 500 mg, conditioned with 10 mL of EtOH and 2 × 10 mL of water). 4-[^{18}F]Fluoroanaline **7a** was eluted from the LiChrolut EN cartridge and through 500 mg of Na_2SO_4 and Celite (3:2 w/w) with THF (1 mL) to give 10.1 ± 1.3 mCi (370 MBq) in 57.5 ± 5.0% dcRCY. A 10 μL aliquot was removed for HPLC analysis (method B), **7a** t_R = 11.4 min. To the **7a**/THF solution was added methyl 8-chloro-8-oxooctanoate (34 μL, 242 μmol), and the mixture was stirred for 5 min at room temperature. A 10 μL aliquot was removed for HPLC analysis (method B), **8a** t_R = 22.8 min. The addition of 250 μL of 50% $NH_2OH_{(aq)}$ and 750 μL of 1 N $NaOH_{(MeOH)}$ and stirring for 3 min provided the desired hydroxamic acid **1a**. A 10 μL aliquot was removed for HPLC analysis (method B), **1a** t_R = 17.0 min. THF and MeOH were evaporated off (50 °C microwave heating under a stream of argon), and the reaction mixture was purified by preparative HPLC (method A), providing 5.1 ± 0.7 mCi (189 MBq) **1a** in 120 ± 12 min, a 39.5 ± 6.0% dcRCY in 97.0 ± 4.7% radiochemical purity over 4 steps and HPLC purification.

Mice. Five Nu/Nu mice received subcutaneous injections with 10^6 A2780 human ovarian cancer cells in Matrigel into each flank and were imaged 10 days later. Mice were anesthetized (Isoflurane 1.5%, O_2 2 L/min) during PET−CT imaging. Therapeutic doses of SAHA (2 mg in 100 μL of 60% PEG400 40% water) were administered ip following initial PET−CT scan and repeated 24 h later. After 48 h from initial therapeutic dose, PET−CT scans were performed again following the iv

administration of **1a**. Ten C57BL/6 mice were used for blood half-life studies. Mice were administered 243 ± 25 μCi of **1a** by tail vein iv injection formulated in 60% PEG400 in water (n = 3), 10% DMSO in water (n = 3), 20% DMAC.Solutol (1:1) in saline (n = 3). In a separate experiment a mouse (n = 1) was administered 265 μCi **1a** by po. Blood sampling was performed by retro-orbital bleed using tared capillary tubes. Samples were weighed, and activity was measured by γ counter. Six C57BL/6 mice were injected with 241 ± 18 μCi **1a** by tail vein iv injection and used to determine biodistribution. Animals were sacrificed at 1 h (n = 3) and 3 h (n = 3) after injection. Tissues were excised and weighed, and activity was measured. Graphpad Prism 4.0c (GraphPad Software Inc., San Diego, CA) was used for regression and statistical analysis. All animal experiments were approved by the Massachusetts General Hospital Institutional Review Committee.

PET-CT. All images were acquired on a Siemens Inveon PET−CT. Each PET acquisition was ∼80 min in duration. PET data were reconstructed from 600 million coincidental 511 keV photon counts on a series of LSO (lutetium oxyorthosilicate) scintillating crystal rings. Counts were rebinned in 3D by registering photons spanning no more than three consecutive rings, then reconstructed into sinograms by utilizing a high resolution Fourier rebinning algorithm. A reconstruction of sinograms yielded a 3D mapping of positron signal using a 2D filtered back-projection algorithm, with a Ramp filter at a Nyquist cutoff of 0.5. Image pixel size was anisotropic, with dimensions of 0.796 mm in the z direction and 0.861 mm in the x and y directions for a total of 128 × 128 × 159 pixels. Calibration of PET signal preceded all scans and was done by scanning an 8.0 cm cylindrical phantom containing a known amount of ^{18}F isotope.

CT was reconstructed from 360 projections of X-rays with a cone beam angle of 9.3° over 360° perpendicular to the animal bed. 80 keV X-rays were transmitted from a 500 μA anode source 347 mm from the center of rotation and recorded on a CCD detector, containing 2048 transaxial and 3072 axial pixels. Projections were calibrated using 70 dark and 70 light images, interpolated bilinearly, processed through a Shepp−Logan filter, then reconstructed using a filtered back projection algorithm. Isotropic CT pixel size was 110.6 μm, with a total of 512 × 512 × 768 pixels. Scaling to Hounsfield units, calibration was done using a 8.0 cm cylindrical phantom containing water prior to CT acquisition.

HDAC Assay. The activity of HDAC inhibitors against individual HDAC isoforms was performed as reported previously.[13]

■ ASSOCIATED CONTENT

Supporting Information. NMR data for compounds **1b** and **8b**. This material is available free of charge via the Internet at http://pubs.acs.org.

■ AUTHOR INFORMATION

Corresponding Author

*For R.W.: phone, 617-643-6133; e-mail, rweissleder@mgh.harvard.edu. For R.M.: phone, 617-643-6286; e-mail, rmazitschek@mgh.harvard.edu.

Author Contributions

†These authors contributed equally.

■ ACKNOWLEDGMENT

Financial support from the NCI (Grants P50CA086355, T32CA079443, and U24CA092782) is gratefully acknowledged. T.R. received a stipend from the Deutschen Akademie der Wissenschaften Leopoldina (Grant LPDS 2009-24).

■ ABBREVIATIONS USED

BLT, Boc-lysine trifluoroacetic acid; DCM, dichloromethane; DMSO, dimethylsulfoxide; DMAC, dimethylacetamide; FAHA, 6-([^{18}F]fluoroacetamide)-1-hexanoicanilide; HDAC, histone deacetylase; HDACi, histone deacetylase inhibitors; HPLC, high-performance liquid chromatography; LC/MS, liquid chromatography−mass spectrometry; nca, no carrier added; PEG, polyethylene glycol; PBS, phosphate buffered saline; PET, positron emission tomography; PET−CT, positron emission tomography−computed tomography; SAHA, suberoylanilide hydroxamic acid; SUV, standardized uptake value; THF, tetrahydrofuran

■ REFERENCES

(1) Haberland, M.; Montgomery, R. L.; Olson, E. N. The many roles of histone deacetylases in development and physiology: implications for disease and therapy. *Nat. Rev. Genet.* **2009**, *10*, 32–42.

(2) Minucci, S.; Pelicci, P. G. Histone deacetylase inhibitors and the promise of epigenetic (and more) treatments for cancer. *Nat. Rev. Cancer* **2006**, *6*, 38–51.

(3) Choudhary, C.; Kumar, C.; Gnad, F.; Nielsen, M. L.; Rehman, M.; Walther, T. C.; Olsen, J. V.; Mann, M. Lysine acetylation targets protein complexes and co-regulates major cellular functions. *Science* **2009**, *325*, 834–840.

(4) Gregoretti, I.; Lee, Y.-M.; Goodson, H. V. Molecular evolution of the histone deacetylase family: functional implications of phylogenetic analysis. *J. Mol. Biol.* **2004**, *338*, 17–31. Haigis, M. C.; Sinclair, D. A. Mammalian sirtuins: biological insights and disease relevance. *Annu. Rev. Pathol.: Mech. Dis.* **2010**, *5*, 253–295.

(5) Richon, V. M.; Webb, Y.; Merger, R.; Sheppard, T.; Jursic, B.; Ngo, L.; Civoli, F.; Breslow, R.; Rifkind, R. A.; Marks, P. A. Second generation hybrid polar compounds are potent inducers of transformed cell differentiation. *Proc. Natl. Acad. Sci. U.S.A.* **1996**, *93*, 5705–5708. Taunton, J.; Hassig, C. A.; Schreiber, S. L. A mammalian histone deacetylase related to the yeast transcriptional regulator Rpd3p. *Science* **1996**, *272*, 408–411.

(6) Shao, Y.; Gao, Z.; Marks, P. A.; Jiang, X. Apoptotic and autophagic cell death induced by histone deacetylase inhibitors. *Proc. Natl. Acad. Sci. U.S.A.* **2004**, *101*, 18030–18035.

(7) Bernstein, B. E.; Meissner, A.; Lander, E. S. The mammalian epigenome. *Cell* **2007**, *128*, 669–681.

(8) Feng, D.; Liu, T.; Sun, Z.; Bugge, A.; Mullican, S. E.; Alenghat, T.; Liu, X. S.; Lazar, M. A. A circadian rhythm orchestrated by histone deacetylase 3 controls hepatic lipid metabolism. *Science* **2011**, *331*, 1315–1319. Zhong, L.; Urso, A. D.; Toiber, D.; Sebastian, C.; Henry, R. E.; Vadysirisack, D. D.; Guimaraes, A.; Marinelli, B.; Wikstrom, J. D.; Nir, T.; Clish, C. B.; Vaitheesvaran, B.; Iliopoulos, O.; Kurland, I.; Dor, Y.; Weissleder, R.; Shirihai, O. S.; Ellisen, L. W.; Espinosa, J. M.; Mostoslavsky, R. The Histone deacetylase Sirt6 regulates glucose homeostasis via Hif1alpha. *Cell* **2010**, *140*, 280–293.

(9) Guan, J.-S.; Haggarty, S. J.; Giacometti, E.; Dannenberg, J.-H.; Joseph, N.; Gao, J.; Nieland, T. J. F.; Zhou, Y.; Wang, X.; Mazitschek, R.; Bradner, J. E.; DePinho, R. A.; Jaenisch, R.; Tsai, L.-H. HDAC2 negatively regulates memory formation and synaptic plasticity. *Nature* **2009**, *459*, 55–60. Kim, D.; Frank, C. L.; Dobbin, M. M.; Tsunemoto, R. K.; Tu, W.; Peng, P. L.; Guan, J.-S.; Lee, B.-H.; Moy, L. Y.; Giusti, P.; Broodie, N.; Mazitschek, R.; Delalle, I.; Haggarty, S. J.; Neve, R. L.; Lu, Y.; Tsai, L.-H. Deregulation of HDAC1 by p25/Cdk5 in Neurotoxicity. *Neuron* **2008**, *60*, 803–817.

(10) de Zoeten, E. F.; Wang, L.; Butler, K.; Beier, U. H.; Akimova, T.; Sai, H.; Bradner, J. E.; Mazitschek, R.; Kozikowski, A. P.; Matthias, P.; Hancock, W. W. Histone deacetylase 6 and heat shock protein 90 control the functions of Foxp3(+) T-regulatory cells. *Mol. Cell. Biol.* **2011**, *31*, 2066–2078. Wang, L.; de Zoeten, E. F.; Greene, M. I.; Hancock, W. W. Immunomodulatory effects of deacetylase inhibitors: therapeutic targeting of FOXP3+ regulatory T cells. *Nat. Rev. Drug Discovery* **2009**, *8*, 969–981.

(11) Patel, V.; Mazitschek, R.; Coleman, B.; Nguyen, C.; Urgaonkar, S.; Cortese, J. F.; Barker, R. H.; Greenberg, E.; Tang, W.; Bradner, J. E.; Schreiber, S. L.; Duraisingh, M. T.; Wirth, D. F.; Clardy, J. Identification and characterization of small molecule inhibitors of a class I histone deacetylase from *Plasmodium falciparum*. *J. Med. Chem.* **2009**, *52*, 2185–2187.

(12) Wiech, N. L.; Fisher, J. F.; Helquist, P.; Wiest, O. Inhibition of histone deacetylases: a pharmacological approach to the treatment of non-cancer disorders. *Curr. Top. Med. Chem.* **2009**, *9*, 257–271.

(13) Bradner, J. E.; West, N.; Grachan, M. L.; Greenberg, E. F.; Haggarty, S. J.; Warnow, T.; Mazitschek, R. Chemical phylogenetics of histone deacetylases. *Nat. Chem. Biol.* **2010**, *6*, 238–243.

(14) Weichert, W. HDAC expression and clinical prognosis in human malignancies. *Cancer Lett.* **2009**, *280*, 168–176.

(15) O'Connor, O. A.; Heaney, M. L.; Schwartz, L.; Richardson, S.; Willim, R.; MacGregor-Cortelli, B.; Curly, T.; Moskowitz, C.; Portlock, C.; Horwitz, S.; Zelenetz, A. D.; Frankel, S.; Richon, V.; Marks, P.; Kelly, W. K. Clinical experience with intravenous and oral formulations of the novel histone deacetylase inhibitor suberoylanilide hydroxamic acid in patients with advanced hematologic malignancies. *J. Clin. Oncol.* **2006**, *24*, 166–173.

(16) Reid, A. E.; Hooker, J.; Shumay, E.; Logan, J.; Shea, C.; Kim, S. W.; Collins, S.; Xu, Y.; Volkow, N.; Fowler, J. S. Evaluation of 6-([(18)F]fluoroacetamido)-1-hexanoicanilide for PET imaging of histone deacetylase in the baboon brain. *Nucl. Med. Biol.* **2009**, *36*, 247–258.

(17) Hooker, J. M.; Kim, S. W.; Alexoff, D.; Xu, Y.; Shea, C.; Reid, A.; Volkow, N.; Fowler, J. S. Histone deacetylase inhibitor MS-275 exhibits poor brain penetration: pharmacokinetic studies of [^{11}C]MS-275 using positron emission tomography. *ACS Chem. Neurosci.* **2010**, *1*, 65–73.

(18) Sankaranarayanapillai, M.; Tong, W. P.; Yuan, Q.; Bankson, J. A.; Dafni, H.; Bornmann, W. G.; Soghomonyan, S.; Pal, A.; Ramirez, M. S.; Webb, D.; Kaluarachchi, K.; Gelovani, J. G.; Ronen, S. M. Monitoring histone deacetylase inhibition in vivo: noninvasive magnetic resonance spectroscopy method. *Mol. Imaging* **2008**, *7*, 92–100.

(19) Lahm, A.; Paolini, C.; Pallaoro, M.; Nardi, M. C.; Jones, P. A.; Neddermann, P.; Sambucini, S.; Bottomley, M. J.; Lo Surdo, P.; Carfi, A.; Koch, U.; De Francesco, R.; Steinkuhler, C.; Gallinari, P. Unraveling the hidden catalytic activity of vertebrate class IIa histone deacetylases. *Proc. Natl. Acad. Sci. U.S.A.* **2007**, *104*, 17335–17340.

(20) Gediya, L. K.; Chopra, P.; Purushottamachar, P.; Maheshwari, N.; Njar, V. C. O. A new simple and high-yield synthesis of suberoylanilide hydroxamic acid and its inhibitory effect alone or in combination with retinoids on proliferation of human prostate cancer cells. *J. Med. Chem.* **2005**, *48*, 5047–5051.

(21) Olma, S.; Ermert, J.; Coenen, H. H. 4-[^{18}F]fluorophenyl ureas via carbamate-4-nitrophenyl esters and 4-[^{18}F]fluoroaniline. *J. Labelled Compd. Radiopharm.* **2006**, *49*, 1037–1050.